Virtual chemistry for temperature and CO prediction in LES of non-adiabatic turbulent flames

Giampaolo Maio, Mélody Cailler, Renaud Mercier, Benoit Fiorina

Virtual chemistry for temperature and CO prediction in LES of non-adiabatic turbulent flames

Giampaolo Maio[a,*], Mélody Cailler[a,b], Renaud Mercier[b], Benoît Fiorina[a]

[a] *Laboratoire EM2C, CNRS, CentraleSupélec, Université Paris-Saclay, 3 rue Joliot Curie 91192 Gif Sur Yvette cedex, France*
[b] *SAFRAN Tech, Rue des Jeunes Bois, Châteaufort - CS 80112, 78772 Magny-les-Hameaux, France*

Abstract

Flames stabilization and pollutant formation in confined combustion chambers are affected by heat losses. Reliable numerical simulations must account for such complex phenomena at a reduced CPU cost. The aim of the present work is the development of a comprehensive reduced chemistry model able to account for the impact of heat losses on chemical flame structure. The recently developed virtual chemistry concept has shown promising capabilities to capture detailed chemistry effects with a reduced set of virtual species and kinetic reactions in adiabatic flame conditions. The approach consists in : i) using a virtual main chemical mechanism coupled to the flow solver equations to predict temperature and heat release, ii) designing satellite submechanisms dedicated to the description of pollutant formation phenomena. The virtual mechanism is trained to recover the properties of an ensemble of target flames. Here burner-stabilized flamelets are introduced in the reference database to capture the influence of heat-losses on flame heat release

*Corresponding author: Giampaolo Maio
Email address: giampaolo.maio@centralesupelec.fr (Giampaolo Maio)

and pollutant formation. The present approach is validated in 1D laminar burner stabilized flames and radiative freely propagating flame configurations. Finally the non adiabatic virtual chemistry is used to perform LES of a premixed turbulent combustion chamber submitted to wall heat losses. Comparison against experiment shows that non adiabatic simulation captures well the flame shape, the temperature and the CO prediction.
Keywords:
Heat losses, Kinetic scheme optimization, Turbulent flames, Large Eddy Simulation

1. Introduction

By reducing the temperature and the flame consumption speed, heat exchanges affect the flame stabilization mechanisms [1, 2] as well as major species and pollutant formation [3]. In addition, combination of heat losses and flow strain effects promote local extinction, at the origin of incomplete fuel consumption [4]. The proper capture of flame heat losses is therefore crucial for numerical simulations of industrial combustion chambers [5].

The task is however challenging as these mechanisms are governed by complex interactions between turbulence and chemistry [6]. As the direct inclusion of detailed chemistry in Large Eddy Simulation (LES) of real scale combustion chambers is prohibitive, three main reduction routes are currently employed [7]: i) Mechanism reduction leading to analytically reduced mechanism [8, 9]. Despite the recent promising application of analytic chemistry to a swirled combustor [10], the computational costs along with numerical stiffness remain restrictive. ii) Chemistry tabulation [7, 11]. Heat

transfers are handled by adding a dedicated coordinate (usually the enthalpy) to the look-up table [12–14]. However tabulated chemistry shows some limitations when the encountered flame structures differ from the tabulated archetypes [15]. Multiple flame archetypes has to be considered, which both complicates the generation of the chemical look-up table [16–18] and causes memory issues [19, 20]. iii) Empirically reduced global mechanisms [21, 22] constitute another CPU efficient strategy, currently used to perform LES of industrial scale combustion chambers [23, 24]. However, these schemes only capture global flame properties on a limited range of operating condition and cannot predict pollutants.

An alternative method called *virtual chemistry* has been recently developed [25, 26] (see S1) to face the above mentioned limitations. This strategy consists in designing a virtual mechanism composed of virtual reactions and virtual species whose thermo-chemical properties are optimized to target "real" flame properties of interest by combustion engineers (such as temperature, pollutant concentration etc.). A virtual main mechanism dedicated to capture the temperature and heat release [25] and a satellite sub-mechanism for CO prediction [26] have been validated in both laminar premixed and non premixed adiabatic configurations. The objective of the present work is to extend both virtual schemes to non-adiabatic configurations in order to perform a LES of turbulent flame submitted to heat losses.

The virtual schemes are developed in Sec 2 and tested in Sec 3 on two configurations: a laminar premixed flame submitted to radiative heat transfers and the semi-industrial Preccinsta turbulent combustion chamber [27]. Both adiabatic and non-adiabatic LES of the Preccinsta combustor are performed

to investigate the capability of the virtual chemistry approach to capture the effect of heat losses on flame shape and CO formation. Finally a mesh refinement analysis is performed to investigate the impact of the turbulent combustion model on the numerical results.

2. Non-adiabatic virtual chemical scheme

As discussed in detail in [26], a virtual chemical scheme is decomposed into a main mechanism and a satellite sub-mechanism dedicated to pollutant formation prediction. Here, the main 2-step mechanism, which aims to predict the heat release and the flame temperature has the following structure:

$$\alpha_F^v F + \alpha_{Ox}^v Ox \rightarrow \alpha_I^v I \tag{R1}$$

$$\alpha_I^v I \rightarrow \sum_{k=1}^{N_P^v} \alpha_{P_k}^v P_k \tag{R2}$$

where α_χ^v are the stoichiometric coefficients per mass unit of the virtual species χ. The symbols F, Ox and I, respectively, represent the fuel, the oxidizer and a virtual intermediate species. The burnt gases composition is modeled by a mixture composed of N_P^v virtual products P_k. A non reactive dilutant species D is added to the virtual mixture having the same thermo-chemical properties as the real species N_2. Real thermo-chemical properties are retained for fuel and oxidizer as well. The following satellite 3-steps mechanism is proposed to predict the CO formation:

$$\alpha_F^v F + \alpha_{Ox}^v Ox \rightarrow \alpha^v CO + (1-\alpha^v)\, V_1 \tag{R3}$$

$$F + V_1 \rightarrow F + CO \tag{R4}$$

$$CO \leftrightarrow V_2 \tag{R5}$$

where V_1 and V_2 are two virtual species.

2.1. Thermochemical equilibrium

2.1.1. Temperature

The thermodynamic properties of each species k is defined by the vector $\psi_k = (c_{p_k}, h_k)$, where c_{p_k} and h_k denote the heat capacity and the enthalpy, respectively. Thermo-chemical equilibrium is recovered if the mixture composed of N_P^v *virtual* species plus the fuel F, the oxidizer Ox and the dilutant D matches the thermodynamic properties given by the reference detailed scheme composed of N_s^d *real* species. This constraint is formalized by the following relation:

$$\sum_{k=1}^{N_s^d} \psi_k^d Y_k^d|^{eq} = \sum_{k=F,Ox,D} \psi_k^v Y_k^v|^{eq} + \sum_{k=1}^{N_p^v} \psi_{P_k}^v Y_{P_k}^v|^{eq} \tag{1}$$

The virtual intermediate species I is fully consumed by reaction R2 and therefore not present at equilibrium. The equality 1 is applied to each equilibrium state of the mixture (characterized at constant pressure, by the equivalence ratio ϕ and enthalpy h) in order to identify the virtual products thermodynamical properties. The reference burnt gas composition $Y_k^d(\phi, \Delta h)$ is given by thermochemical equilibrium computations, where $\Delta h = h^{ad} - h$ is the enthalpy defect with respect to adiabatic conditions h^{ad}.

ψ_k is in practice modeled by a JANAF [28] temperature dependent polynomial functions of coefficient $a_{l,k}$, suitable for ideal gas states. By identifying each polynomial term, Eq 1 is then recast into the following system of equations for each state of the mixture:

$$\sum_{k=1}^{N_p^v} a_{lP_k}^v \alpha_{Pk} = \sigma_l(\phi, \Delta h)/Y_P^v \quad \text{for} \quad l = 1, ..., 6 \tag{2}$$

where $\sigma_l(\phi, \Delta h) = \sum_{k=1}^{N_s^d} a_{lk}^d Y_k^d - \sum_{k=F,Ox,D} a_{lk}^v Y_k^v$. Y_P^v is the total mass fraction of virtual products and $Y_{P_k}^v = \alpha_{Pk} Y_P^v$ where α_{Pk} are the product stoichiometric coefficients per mass unit.

The strategy to recover the equilibrium thermodynamical state for all equivalence ratio ϕ and enthalpy defect Δh conditions consists in the two following steps:

- *Equilibrium temperature under adiabatic conditions.* For that purpose, as detailed in [25], the number of virtual species N_P^v, the stoichiometric coefficients $\alpha_{P_k}^v(\phi)$ and the thermodynamic properties ψ_k^v of virtual products are optimized to satisfy Eq. 2 for $\Delta h = 0$ with the arbitrary constraint $\sum_{k=1}^{N_p^v} \alpha_{Pk}(\phi) = 1$. For methane/air combustion, an accurate estimation of the adiabatic flame temperature is obtained with four virtual products, i.e. with $N_p^v = 4$.
- *Equilibrium temperature under non-adiabatic conditions.* The number of virtual species N_P^v and their thermo-properties ψ_k^v identified under adiabatic conditions are conserved. A dependency on enthalpy defect is added to the stoichiometric coefficients ($\alpha_{Pk}(\phi, \Delta h)$) to satisfy Eqs. 2. This formalism adapts the virtual species composition to mimic the "real" thermo-chemical equilibrium state dependency to heat losses.

Figure 1a shows that the non-adiabatic flame temperature is indeed well retrieved by a virtual product mixture composed by 4 species over a wide range of equivalence ratio and enthalpy defect conditions.

2.1.2. CO mass fraction

The CO mass fraction at equilibrium is given by the equilibrium constant $K_{c,5}^v$ [26] of the reversible reaction $R5$. Function of equivalence ratio for

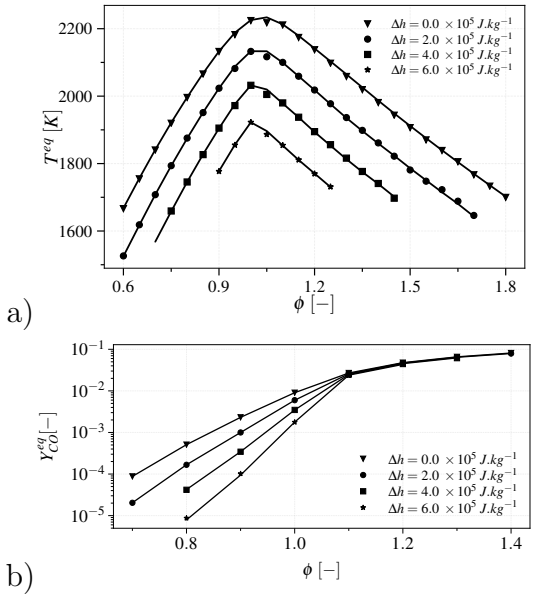

Figure 1: Non-adiabatic equilibrium temperature (a) and equilibrium CO mass fraction (b) versus equivalence ratio for different enthalpy defects, where $\Delta h = 0$ corresponds to adiabatic conditions. The mixture is composed of methane and air at an initial temperature of 300 K under atmospheric pressure conditions. Lines is the reference detailed thermochemical equilibrium solution obtained with 53 species whereas the symbols are the virtual chemistry prediction.

adiabatic condition, a dependency on the enthalpy defect is added as follows to account for heat losses:

$$K_{c,5}^{v}\left(\phi, \Delta h\right) = \frac{\left[V_2\right]^{v} |^{eq}\left(\phi, \Delta h\right)}{\left[CO\right]^{d} |^{eq}\left(\phi, \Delta h\right)} \tag{3}$$

where $\left[CO\right]^{d} |^{eq}\left(\phi, \Delta h\right)$ is obtained from reference thermochemic equilibrium computations. As V_1 is entirely consumed in the burnt gases, $\left[V_2\right]^{v} |^{eq}(\phi)$ is deduced from mass conservation. As shown in Fig.1b, the equilibrium predicted by virtual CO sub-mechanism agrees with complex detailed chemistry equilibrium computations.

2.2. Chemical kinetics

2.2.1. Heat release and flame consumption speed

The rate of progress of reactions R1 and R2 reads:

$$q_1 = A_1(\phi, \Delta h) \exp\left(\frac{-E_{a,1}}{RT}\right) [F]^{F_{F,1}} [O]^{F_{Ox,1}} \tag{4}$$

$$q_2 = A_2 \exp\left(\frac{-E_{a,2}}{RT}\right) [I]^{F_{I,2}(\phi,\Delta h)} \tag{5}$$

where A_r and $E_{a,r}$ are the pre-exponential factor and activation energy of reaction r, respectively, A_1 and $F_{I,2}$ being both function of equivalence ratio and heat losses. $F_{k,r}$ is the k-th species reaction order for the reaction r and $[k]$ is the k-th species molar concentration. All these parameters are optimized by using a genetic algorithm in order to minimize the following fitness function:

$$f_{kinetic}^{main}(A_r, E_{a,r}, F_{k,r}) = \sum_{j=1}^{N_c} w_1 \frac{|S_{L_j}^v - S_{L_j}^d|}{S_{L_j}^d} + w_2 \frac{\|T_j^v(x) - T_j^d(x)\|_{L_2}}{\|T_j^d(x)\|_{L_2}}, \tag{6}$$

where S_{L_j} and $T_j(x)$ are the laminar flame consumption speed and the temperature profile of the j^{th} set of operating conditions $(\phi, \Delta h)$. The weights w_1 and w_2 are imposed equal to 0.01 and 0.99, respectively, to give appropriate influence to both criteria.

The optimization of kinetic rate parameter $(A_r, E_{a,r}, F_{k,r})$ is first performed by targeting a set of adiabatic freely-propagating 1D flames computed with the GRI 3.0 [29] detailed mechanism [25, 26]. Then, to identify the dependency on A_1 and $F_{I,2}$ to heat losses, a second optimization step is realized by targeting non-adiabatic flamelets. The archetype retained for

that purpose is the 1-D burner stabilized flame configuration, used in many non-adiabatic chemistry tabulation methods [12, 13, 30]. By acting on the fresh gases mass flow rates, the range of enthalpy defect is covered from adiabatic ($\Delta h = 0$) up to the extinction limit ($\Delta h = \Delta h^q$). During the optimization step, the objective function $f_{kinetic}^{main}$ is computed through Eq. 6 by using the following definition of flame consumption speed, valid in both freely-propagating and burner-stabilized flame configurations [30]:

$$S_l = \frac{1}{\rho^f (Y_F^{eq} - Y_F^n)} \left(\int_0^{+\infty} \rho \dot{\omega}_F \left(x, \phi, \Delta h\right) dx + J_F^n \right) \tag{7}$$

where Y_F^{eq} and Y_F^n are the fuel mass fractions respectively in the fully burnt gases and at the burner nozzle. J_F^n is the molecular diffusive flux of fuel at the burner nozzle. Note that here $\Delta h^q(\phi)$ is defined for $S_l(\phi) = 5$ cm.s^{-1}.

A series of burner stabilized flames computed at $\phi = 0.8$ with the non-adiabatic virtual scheme are compared against detailed chemistry solutions in Fig 2 for three ratios $\Delta h / \Delta h^q$. With only 4 virtual species and 2 virtual reactions the temperature profiles are fairly reproduced by the detailed chemistry prediction which includes 53 species and 325 reactions. As shown in Fig 3, the flame consumption speed given by Eq. 7, *a posteriori* predicted by the non-adiabatic virtual mechanism, compares well against the detailed chemistry reference solution. Burner stabilized flames are also computed with the original adiabatic virtual mechanism developed in [25, 26]. In this last case, the flame consumption speed shown by empty circles in Fig.3 presents significant bias increasing with Δh. Indeed, as the adiabatic formulation of the virtual chemistry involves temperature dependent reaction rates, a sensitivity of the flame speed to the mixture enthalpy is expected. However, as shown in Fig. 3, the prediction is not accurate and the non-adiabatic

developments correct this mis-prediction.

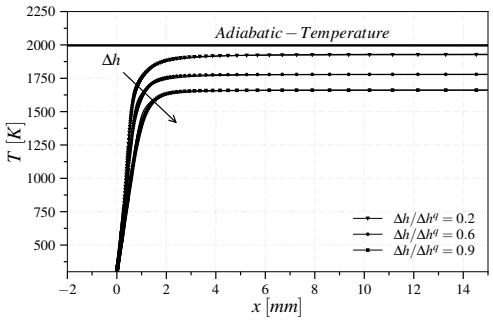

Figure 2: Temperature profiles computed for burner stabilized flames at $\phi = 0.8$. Δh is normalized using the quenching maximum value ($5.7 \times 10^5 J.kg^{-1}$). Lines: detailed chemistry solutions. Symbols: virtual chemistry solutions.

2.2.2. CO formation

The rate of progress of reactions R3, R4 and R5 are modeled by retaining the formulation along with the adiabatic kinetic rate parameters proposed in [26]. Extension to heat losses and equivalence ratio is achieved by applying the optimization procedure developed for the main mechanism and described in section 2.2.1, with pre-exponential constants $A_3(\phi, \Delta h)$, $A_4(\phi, \Delta h)$ and $A_5(\phi, \Delta h)$ tabulated in terms of both equivalence ratio and enthalpy defect. For the optimization process, the burner-stabilized flame archetype is retained to constitute the target database with a fitness function based on the CO mass fraction profiles [26].

Figure 4 compares, for a 1-D burner stabilized flame at fixed ϕ and enthalpy defect, the computed CO mass fractions profiles obtained with the non-adiabatic virtual scheme and with the adiabatic one versus the reference solution. Significant differences are observed between the two solutions

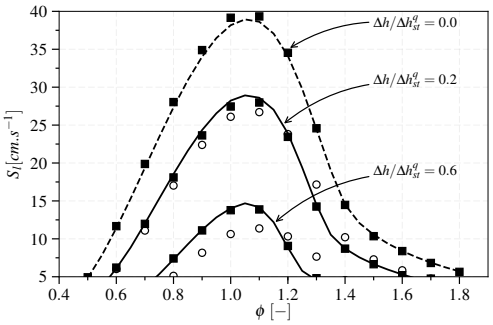

Figure 3: Laminar flame consumption speed computed on freely propagating adiabatic (dashed-line) and burner stabilized (solid line) configurations versus equivalence ratio for different enthalpy defects. Δh is normalized using the quenching maximum value at stoichiometry ($8.1 \times 10^5 J.kg^{-1}$). Lines: detailed chemistry. Squares: non-adiabatic virtual chemical scheme. Empty circle: adiabatic virtual scheme.

demonstrating the value of the developments. In particular, the influence of heat losses on the Y_{CO} peak is well predicted only with non adiabatic scheme.

3. Results

3.1. 1D radiative flames

The non-adiabatic virtual schemes are challenged on 1D laminar premixed flames submitted to radiative heat losses, which have not been considered during the optimization step. Radiative fluxes modeled by $\dot{q} = \epsilon\sigma(T^4 - T_0^4)$ are added to the energy balance equation of the 1-D flame solver REGATH [31]. σ is the Stefan-Boltzmann constant, ϵ the gas emissivity, T is the local gas temperature and T_0 the fresh gases temperature. Detailed chemistry simulations performed with this basic radiative model will serve as a reference. Even not realistic, this crude radiative model is however sufficient to

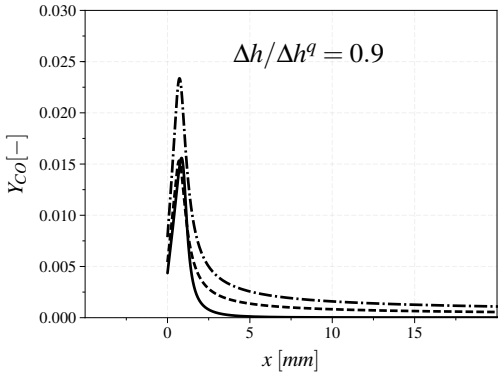

Figure 4: CO mass fractions profiles computed for a burner stabilized flame at $\phi = 0.8$ and at fixed $\Delta h/\Delta h^q$. Continuous line: Detailed chemistry calculations. Dashed dot line: Adiabatic virtual chemistry calculation. Dashed line: Non adiabatic virtual chemistry calculations.

verify the ability of non adiabatic virtual chemistry to capture the impact of radiative heat losses on the chemical flame structure.

Figures 5a and 5b compare temperature and Y_{CO} predicted by detailed and virtual chemistry for different values of gas emissivity ε. Temperature comparisons show reasonably good agreement between virtual and detailed chemistry, with small discrepancies observed for high emissivity values. The flame front is not affected by radiative heat losses and consequently all CO profiles converge toward the ones obtained for $\varepsilon = 0$ (i.e. no radiative flame). Looking to the post flame region instead, radiative heat losses affect the burnt gases composition and virtual chemistry predicts the CO production.

As an intermediate conclusion, the virtual chemical scheme still perform well in non-adiabatic configurations not included in the target learning database. This confirms that enthalpy variations act identically on the chemical flame structure regardless of the origin of heat losses as observed in [13].

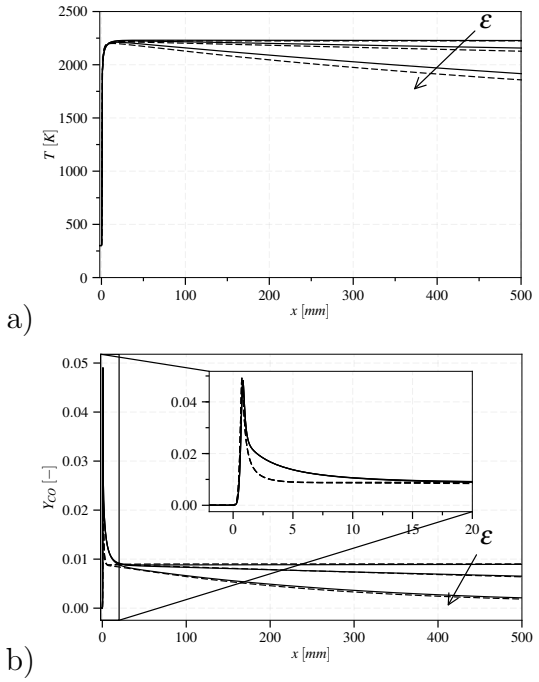

Figure 5: Temperature and CO mass fraction profiles for a series of 1D stoichiometric premixed laminar flame submitted to radiative heat losses for 3 different values of gas emissivity, respectively, $\varepsilon = 0.0$, $\varepsilon = 0.1$, $\varepsilon = 0.5$. A zoom close to the flame region is done for CO mass fraction profiles. Continuous lines: detailed chemistry. Lines with symbols: non adiabatic virtual chemistry.

3.2. LES of a non-adiabatic turbulent premixed flame

The virtual chemistry is used to simulate the Preccinsta combustor made of a plenum, a swirler and a combustion chamber [27]. The combustion chamber is directly fed with a premixed mixture ($\phi = 0.83$) at a constant mass flow rate $\dot{m} = 12.9\, g.s^{-1}$.

Many numerical simulations of this configuration have been conducted to validate LES turbulent combustion models [32–39]. All these simulations reproduce fairly well the flow dynamics as well as the mean flame front po-

sition but fail to predict the flame temperature and CO production in the outer recirculation zone. These differences are attributed to the adiabatic wall assumption not representative of the real experimental conditions where convective heat transfers occur through the injector system and quartz windows. As the wall temperature was not measured experimentally, a trial and error procedure based on non-adiabatic computation with a 17 species skeletal scheme [40] has been conducted in [41]. Wall temperature Dirichlet boundary conditions have been identified to match the experimental measurements of temperature and the species in the near wall region. The imposed wall temperature profile is shown in Fig 6

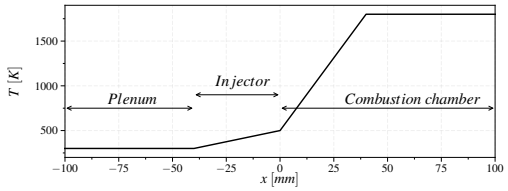

Figure 6: Wall temperature profiles imposed along the flame side wall chamber [41].

Two unstructured grids are used in the present simulations: a coarser grid made of 2.7 millions of nodes and a finer one composed of 20.9 millions of nodes. LES are performed using the YALES2 low-Mach number, unstructured finite volume flow solver [42]. A fourth-order temporal scheme is used to perform time integration of convective terms while a centered fourth-order scheme is used for spatial discretization. The sub-grid Reynolds stresses tensor is closed using the WALE model [43]. Combustion chemistry is modeled using the above described non adiabatic virtual mechanism solving both the two-step main mechanism and the CO dedicated sub-mechanism. Virtual

chemistry is coupled with turbulence using the Thickened Flame model for LES (TFLES) [44]. A flame sensor dedicated to virtual chemistry is used [45]. The Charlette model [46] is used to close the subgrid scale flame wrinkling, setting the constant parameter $\beta = 0.5$. The three following simulations are performed: adiabatic on the coarse grid (AC), non-adiabatic on the coarse grid (NAC) and non-adiabatic on the fine grid (NAF).

Non-adiabatic virtual chemistry predicts very well the mean and RMS temperature profiles shown in Fig. 7. In particular, the comparison between AC and NAC demonstrates that accounting for heat losses clearly improves both mean and RMS temperature predictions in the near wall region, where the outer recirculation zone is located. The predicted chem-

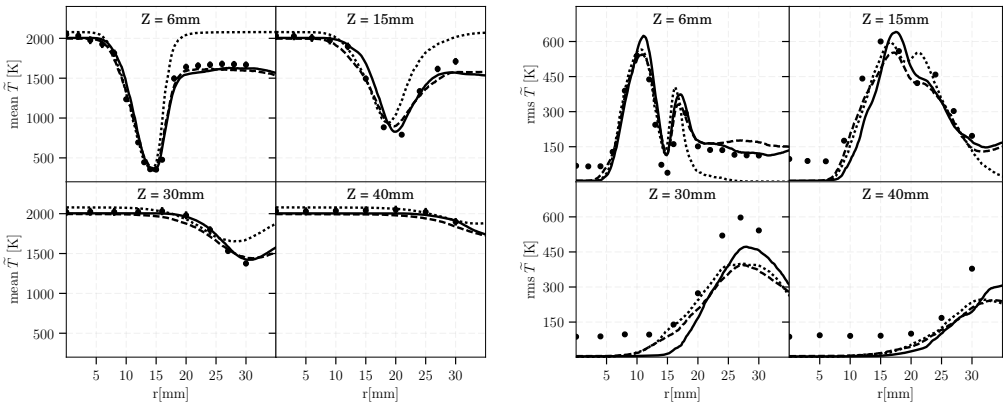

Figure 7: Mean and rms temperature radial profiles at several axial locations from the injector. Circle: Experimental data with the corresponding experimental error bar. Squared dotted lines: AC results. Dashed lines: NAC results. Continuous lines: NAF results.

ical flame structure, illustrated by instantaneous snapshots of filtered CO mass fraction shown in Fig. 9, differs significantly whether or not heat losses are considered. Unlike to experimental OH-LIF and OH-chemiluminescence

measurements [27], AC predicts a M-shape flame. The heat losses included in NAC induce a thinner outer branch of the flame and local flame extinctions in the outer recirculation zone. This observation is confirmed in NAF where the flame resolution is improved. A V-shape flame is retrieved, accordingly to experimental observation. This information is confirmed in Fig. 8. where a qualitative comparison between OH-chemiluminescence and mean computed heat release is proposed.

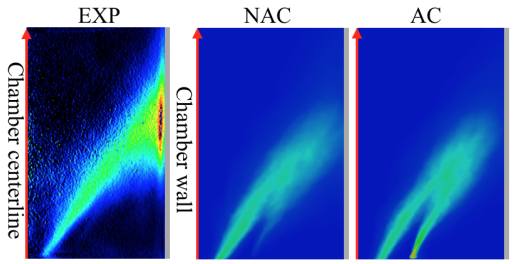

Figure 8: Qualitative comparison between experimental OH chemiluminescence and computed mean heat release for NAC and AC simulations. The heat release rate is normalized between 0 and $1 \times 10^9\ W.m^{-3}$.

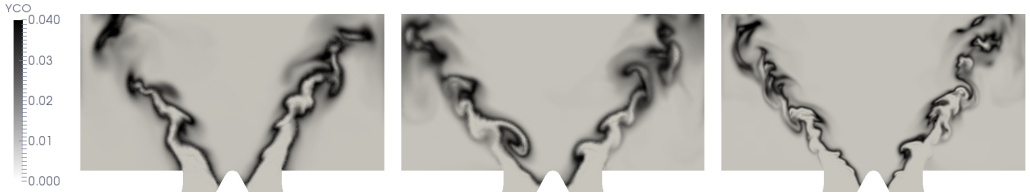

Figure 9: Instantaneous CO filtered mass fraction snapshot on the middle-plane of the combustion chamber. From left to right: AC, NAC, NAF.

Mean CO mass fraction are compared in Fig. 10. Adiabatic simulation overestimates the CO production in the outer recirculation zone. In particular a peak of CO, not observed in the experiments, is predicted in AC at

(r=17 mm; Z= 6 mm) and (r=22 mm; Z= 15 mm). The amplitude of this peak is drastically reduced by NAC which accounts for the impact of heat losses on the CO chemistry. The simulations using the virtual chemistry approach however still overestimates the peak of CO .

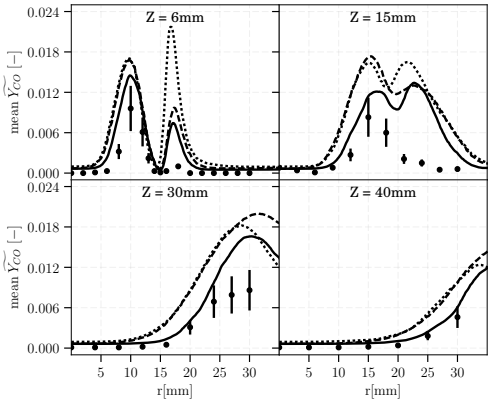

Figure 10: Mean CO mass fraction radial profiles at several axial locations from the injector. Circle: Experimental data with the corresponding experimental errorbar. Squared dotted lines: AC results. Dashed lines: NAC results. Continuous lines: NAF results.

This undesirable behavior is due to the artificial thickening of the flame front. To demonstrate this spurious effect, the 1-D structure of a mean flame brush is manufactured from a random distribution of 100,000 1-D flamelet solutions, as proposed by Vervisch *et al.* [47]. The distribution of flamelet positions is adjusted to recover the PRECCINSTA mean flame brush thickness that is estimated to be about 5 mm at the first axial measurement (z=6 mm). The Reynolds averaging of this flamelets ensemble provides a reference mean CO mass fraction solution, shown in solid line in Fig. 11. The solution expected by the TFLES approach is also manufactured by randomly distributing a set of 1-D thickened flames. The Reynolds averaging of this ensemble

of thickened flamelets is also performed. Results are plotted in Fig. 11 for the values F=4.5 and F= 2.25, which corresponds to the maximum values of flame thickening factors computed in coarse and fine meshes at z= 6 mm, respectively. (dashed and dotted lines). The comparison between mean reference and thickened CO profiles shows that TFLES overestimates the peaks of mean intermediate species. The overestimation increases with F. As observed in Fig. 11, refining the mesh enable to decrease the thickening factor and limits its spurious influence on the species production.

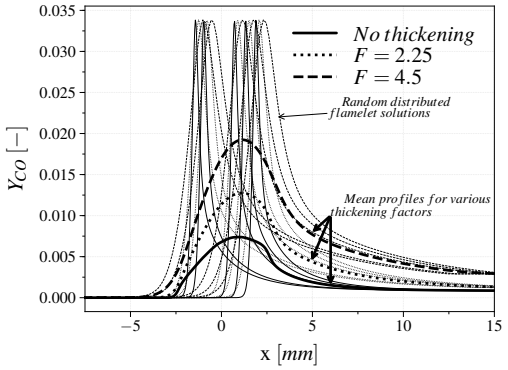

Figure 11: Thin lines: Some of the random distributed flamelet solutions for the various thickening factors. Bold lines: Reynolds averaged mean profiles for the corresponding thickening factors.

4. Conclusion

Virtual chemistry has been extended to account for the effect of heat losses on flame global quantities (temperature and laminar flame speed) and CO prediction. The validity domain of the model has been enlarged without adding species and reactions to the reduced schemes. Detailed chemistry

phenomena are well reproduced in non adiabatic premixed laminar flame simulations. The virtual non adiabatic scheme is coupled with the TFLES turbulent combustion model to perform an LES of the Preccinsta chamber. The comparison between adiabatic and non adiabatic results shows a significant improvement in flame shape prediction, temperature and CO mass fraction fields. Non adiabatic simulations predicts a V shape like flame which is closer to the experimental observations.

Discrepancies in CO mass fraction prediction are first attributed to the artificial thickening of the flame front. However the chemical flame structure is also sensitive to strain effects [2] which are not considered here. An improvement would be to enlarge the reference database used to train the virtual chemical scheme by adding for instance strained flamelets.

Future work will focus on extending virtual chemistry methodology for the predictions of other complex pollutants such as NOx and soot precursors.

Acknowledgments

The authors thank Prof. W. Meier for providing experimental data. Pierre Bénard, Vincent Moureau and Ghislain Lartigue from CORIA lab, and the SUCCESS scientific group are acknowledged for providing the YALES2 code and for sharing Preccinsta geometry, mesh and boundary conditions. This project has received funding from the European Unions Horizon 2020 research and innovation programme under the Marie Sklodowska-Curie grant agreement No 643134. This work was granted access to the HPC resources of CINES under the allocations $A0012B00164$ and $A0032B10253$ made available by GENCI (Grand Equipement National de Calcul Intensif)

[1] B. Fiorina, R. Mercier, G. Kuenne, A. Ketelheun, A. Avdić, J. Janicka, D. Geyer, A. Dreizler, E. Alenius, C. Duwig, et al., Combust. Flame 162 (2015) 4264–4282.

[2] R. Mercier, T. Guiberti, A. Chatelier, D. Durox, O. Gicquel, N. Darabiha, T. Schuller, B. Fiorina, Combust. Flame 171 (2016) 42–58.

[3] C. Jainski, M. Rißmann, B. Böhm, J. Janicka, A. Dreizler, Combust. Flame 183 (2017) 271–282.

[4] T. F. Guiberti, D. Durox, L. Zimmer, T. Schuller, Combust. Flame 162 (2015) 4342–4357.

[5] F. Proch, A. Kempf, Proc. Combust. Inst. 35 (2015) 3337–3345.

[6] S. B. Pope, Proc. Combust. Inst. 34 (2013) 1–31.

[7] B. Fiorina, D. Veynante, S. Candel, Flow, Turbulence and Combustion 94 (2015) 3–42.

[8] T. Lu, C. K. Law, Combust. Flame 154 (2008) 761–774.

[9] P. Pepiot-Desjardins, H. Pitsch, Combust. Flame 154 (2008).

[10] T. Jaravel, E. Riber, B. Cuenot, G. Bulat, Proc. Combust. Inst. 36 (2017) 3817–3825.

[11] J. A. V. Oijen, A. Donini, R. J. M. Bastiaans, J. H. M. T. Boonkkamp, L. P. H. D. Goey, Prog. Energy and Combust. Sci. 57 (2016) 30–74.

[12] J. Van Oijen, F. Lammers, L. De Goey, Combust. Flame 127 (2001) 2124–2134.

[13] B. Fiorina, R. Baron, O. Gicquel, D. Thevenin, S. Carpentier, N. Darabiha, et al., Combustion Theory and Modelling 7 (2003) 449–470.

[14] M. Ihme, H. Pitsch, Physics of Fluids 20 (2008) 055110.

[15] B. Fiorina, O. Gicquel, L. Vervisch, S. Carpentier, N. Darabiha, Combust. Flame 140 (2005) 147–160.

[16] V. Bykov, U. Maas, Combust. Theor. Modell. 11 (2007) 839–862.

[17] P. Nguyen, L. Vervisch, V. Subramanian, P. Domingo, Combust. Flame 157 (2010) 43–61.

[18] B. Franzelli, B. Fiorina, N. Darabiha, Proc. Combust. Inst. 34 (2013) 1659–1666.

[19] M. Ihme, A. L. Marsen, H. Pitsch, Journal of Neural Computation 20 (2007) 1–29.

[20] D. Veynante, B. Fiorina, P. Domingo, L. Vervisch, Combust. Theor. Modell. (2008) In Press.

[21] C. K. Westbrook, F. L. Dryer, Combust. Sci. Techol. 27 (1981) 31–43.

[22] W. Jones, R. Lindstedt, Combust. Flame 73 (1988) 233–249.

[23] S. Berger, S. Richard, F. Duchaine, G. Staffelbach, L. Gicquel, Applied Thermal Engineering 103 (2016) 1450–1459.

[24] B. Franzelli, E. Riber, M. Sanjosé, T. Poinsot, Combust. Flame 157 (2010) 1364–1373.

[25] M. Cailler, N. Darabiha, D. Veynante, B. Fiorina, Proc. Combust. Inst. (2017).

[26] M. Cailler, N. Darabiha, B. Fiorina, Submitted (see supplementary material S1) (2018).

[27] W. Meier, P. Weigand, X. R. Duan, R. Giezendanner-Thoben, Combust. Flame 150 (2007) 2–26.

[28] M. W. Chase, J. Curnutt, H. Prophet, R. McDonald, A. Syverud, Journal of physical and chemical reference data 4 (1975) 1–176.

[29] G. P. Smith, D. M. Golden, M. Frenklach, B. Eiteener, M. Goldenberg, C. T. Bowman, R. K. Hanson, W. C. Gardiner, V. V. Lissianski, Z. W. Qin (2011).

[30] R. Mercier, P. Auzillon, V. Moureau, N. Darabiha, O. Gicquel, D. Veynante, B. Fiorina, Flow, turbulence and combustion 93 (2014) 349–381.

[31] N. Darabiha, Combust. Sci. Techol. 86 (1992) 163–181.

[32] B. Franzelli, E. Riber, L. Y. Gicquel, T. Poinsot, Combust. Flame 159 (2012) 621–637.

[33] S. Roux, G. Lartigue, T. Poinsot, U. Meier, C. Bérat, Combust. Flame 141 (2005) 40–54.

[34] G. Albouze, T. Poinsot, L. Gicquel, Comptes Rendus Mécanique 337 (2009) 318–328.

[35] V. Moureau, P. Domingo, L. Vervisch, Combust. Flame 158 (2011) 1340–1357.

[36] P. Wang, N. Platova, J. Fröhlich, U. Maas, International Journal of Heat and Mass Transfer 70 (2014) 486–495.

[37] R. Mercier, V. Moureau, D. Veynante, B. Fiorina, Proc. Combust. Inst. 35 (2015) 1359–1366.

[38] P. S. Volpiani, T. Schmitt, D. Veynante, Combust. Flame 180 (2017) 124–135.

[39] B. Fiorina, R. Vicquelin, P. Auzillon, N. Darabiha, O. Gicquel, D. Veynante, Combust. Flame 157 (2010) 465–475.

[40] R. Sankaran, E. R. Hawkes, J. H. Chen, T. Lu, C. K. Law, Proc. Combust. Inst. 31 (2007) 1291–1298.

[41] P. Benard, R. Mercier, G. Lartigue, V. Moureau, Submitted Proc. Combust. Inst. (2018).

[42] V. Moureau, P. Domingo, L. Vervisch, Comptes Rendus Mécanique 339 (2011) 141–148.

[43] F. Nicoud, F. Ducros, Flow, turbulence and Combustion 62 (1999) 183–200.

[44] O. Colin, F. Ducros, D. Veynante, T. Poinsot, Physics of Fluids (1994-present) 12 (2000) 1843–1863.

[45] M. Cailler, R. Mercier, V. Moureau, D. Nasser, B. Fiorina, 55th AIAA Aerospace Sciences Meeting, AIAA SciTech Forum (2017).

[46] F. Charlette, C. Meneveau, D. Veynante, Combust. Flame 131 (2002) 159–180.

[47] L. Vervisch, P. Domingo, G. Lodato, D. Veynante, Combustion and Flame 157 (2010) 778–789.